Self-trapping of active particles induced by non-reciprocal interactions in disordered media

Rodrigo Saavedra[1,*] and Fernando Peruani[2,†]

[1] *Departamento de Ciencias de la Computación, Centro de Investigación Científica y de Educación Superior de Ensenada, Baja California, México*

[2] *Laboratoire de Physique Theéorique et Modélisation, CNRS UMR 8089, CY Cergy Paris Université, Cergy-Pontoise Cedex, France*

(Dated: April 18, 2024)

Abstract

Disordered media is known to modify the transport properties of active matter depending on interactions between particles and with the substrate. Here we study systems of active particles with visual-like perception that co-align with the positions of perceived conspecifics, and anti-align with positions of static obstacles. We report a novel self-trapping mechanism of particles forming closed loops that progressively shrink, surrounding one or multiple obstacles. This mechanism corresponds to a pinning behavior preventing particle diffusion. Increased co-alignment strength is found to reduce loop shrinking time, although this effect reaches a plateau at higher strengths. Loops are found to initially exhibit local polar order, but eventually they transition to nematic states as they absorb more particles. We show a phase diagram demonstrating self-trapping occurs within a specific range of aperture angles of the vision cone.

Most examples of natural systems, if not all, where collective motion occurs in the wild, take place in heterogeneous media. Examples can be found at all scales. Microtubules driven by molecular motors form complex patterns inside the cell where the space is filled by organelles and vesicles [1, 2]. Bacterial colonies exhibit complex collective behaviors, e.g. swarming in heterogeneous environments such as the soil [3, 4] or highly complex tissues such as in the gastrointestinal tract [5–7]. At a larger scale, herds of mammals migrate long distances traversing rivers, forests, etc. [8, 9]. In active matter, the influence of static obstacles on the collective behavior has been a focus of research in recent years. For example, when velocity alignment is considered, it has been found that a single small obstacle can have a dramatic impact in the large-scale dynamics of polar flocks, leading to flow reversals and chaotic dynamics [10]. In the presence of several randomly placed obstacles, the system becomes disorganized overall, with some of the particles aggregating into small independent clusters [11, 12]. For coupled arrays of active particles, e.g. active polymers, it has been found that they can either rectify or segregate when navigating in porous media [13–15]. Non-reciprocal interactions pertains to a new class of active matter that can be found in system interacting via chemotaxis, hydrodynamic forces, or quorum-sensing [16]. It has been recently explored in theoretical studies [17–21], as well as in particle-based numerical simulations, e.g. in models of particles that move according to positional-based interactions while considering conspecifics located within a restricted cone of vision [22–27]. This mechanism, fundamentally different from the celebrated Vicsek rule, has been successfully applied to describe the collective dynamics of sheep [28, 29], and to induce cohesive group formation in swarms of light-activated colloids [30–32].

In this work, we consider the impact that a heterogeneous medium, i.e. quenched disorder [33–36], may have on collective dynamics of active particles with non-reciprocal interactions. We investigate a new mechanism of self-trapping of active particles forming a loop around static obstacles. This behavior is found to emerge from interactions of particles with visual-like perception combined with positional-based co-alignment between moving particles, as well as anti-alignment between particles and static obstacles. We find trapped loops consist of active particles that remain tangentially oriented in the loop with small fluctuations in the orientation given by thermal diffusion. Once formed, loops can absorb other incoming particles in the system, and also some of the particles can escape due to thermal diffusion. As a result of the increasing number of particles in the loop, the local order of the structure transitions from polar to nematic. We characterize the trapped loops in terms of dynamic parameters like the radius of gyration and mean-squared displacement, as well as distributions for cluster size and displacement. Our analysis shows that self-trapping corresponds to pinning behavior preventing particle diffusion. It is found to induce an exponential decay in the cluster size distribution for small clusters, with a delta peak at larger sizes, and also a quadratic dependence in the displacement probability-density function for small displacements with a range corresponding to the loop size. A phase diagram is also obtained for varying values of the aperture angles of the vision cone, showing that trapping occurs only for intermediate values of the parameters. We also study the emergence of nematic bands that percolate while avoiding the obstacle configuration, or they can self-trap forming a closed loop surrounding multiple obstacles. Our study sheds light to the understanding of active matter with non-reciprocal interactions, including the effect of crowded environments on the collective behavior and transport properties.

Model.–We consider a system of N motile particles and N_o static obstacles distributed inside of a square box of length L. The motion of each motile particle i is governed by

$$\dot{\boldsymbol{r}}_i = v_0 \boldsymbol{e}_i, \tag{1a}$$

$$\dot{\theta}_i = \tau_i^{\mathrm{att}}(\{\boldsymbol{r}_j\}) + \tau_i^{\mathrm{rep}}(\{\boldsymbol{r}_o\}) + \xi_i. \tag{1b}$$

Here v_0 and $\boldsymbol{e}_i = (\cos\theta, \sin\theta)^T$ are the self-propulsion magnitude and direction, ξ_i is a noise term sampled from a normal distribution of width $\sqrt{2D_\theta}$, where D_θ is the rotational

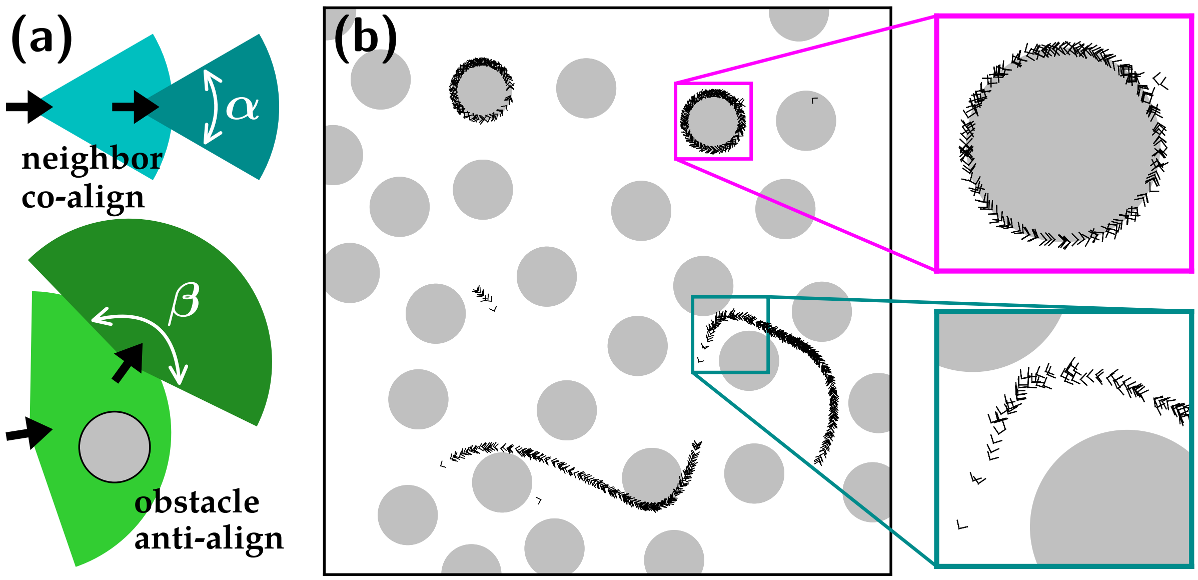

FIG. 1. (a) Illustration of alignment interactions given by Eqs. (2). Each active particle perceives neighbors within a narrow cone of vision of angle α, and obstacles within a wide cone of vision of aperture β. (b) Representative snapshot for a configuration of $N = 900$ particles and $N_o = 30$ static obstacles. Simulation parameters are $\alpha = 0.3$, $\beta = 0.6$, $\sqrt{2D_\theta} = 0.3$.

diffusion coefficient; the terms $\tau_i^{\mathrm{att}}(\{\boldsymbol{r}_j\})$, $\tau_i^{\mathrm{rep}}(\{\boldsymbol{r}_o\})$ correspond to alignment torques induced by neighbour particles j and obstacles o, respectively. They are given by

$$\tau_i^{\mathrm{att}}(\{\boldsymbol{r}_j\}) = -\frac{\gamma^{\mathrm{att}}}{n^{\mathrm{att}}} \sum_{j \in V_i^{\mathrm{att}}} \sin(\beta_{ij} - \theta_i), \tag{2a}$$

$$\tau_i^{\mathrm{rep}}(\{\boldsymbol{r}_j\}) = -\frac{\gamma^{\mathrm{rep}}}{n^{\mathrm{rep}}} \sum_{o \in V_i^{\mathrm{rep}}} \sin(\beta_{io} - \theta_i), \tag{2b}$$

with β_{ij} the polar angle of the vector $\boldsymbol{r}_{ij} = \boldsymbol{r}_j - \boldsymbol{r}_i$, and similarly for β_{io}. Coefficients γ^{att}, γ^{rep} are attraction and repulsion alignment strengths, respectively; V_i^{att}, V_i^{rep} are interaction zones satisfying $V_i^{\mathrm{att}} \in V_i^{\mathrm{rep}}$. The interaction zone V_i^{att} corresponds to a cone of vision of aperture angle α, and V_i^{rep} to a cone of vision of angle β, see Fig. 1a. Each term is normalized by n^{att}, n^{rep} the number of neighbours within each interaction region.

We consider a configuration of homogeneously distributed obstacles, separated by a distance d. As we increase the number of obstacles N_o, d decreases as well. The effective obstacle size is given by the interaction with the active particles, which have an interaction range cutoff r_{cut}. Therefore, obstacles overlap occur only when $d < 2r_{\mathrm{cut}}$. We perform particle-based numerical simulations by solving Eq. 1 for $N = 900$ particles randomly distributed within a square box of side length $L = 30$, with fixed self-propulsion speed $v_0 = 1$, alignment strengths $\gamma^{\text{att}} = -\gamma$, $\gamma^{\text{rep}} = \gamma$ with $\gamma = 5$, and cone of vision range of $r_{\text{cut}} = 1.5$. We choose two different sets of parameters for (α, D_θ). One set with $\alpha/\pi = 0.3$ and $\sqrt{2D_\theta} = 0.3$ where particles are known to aggregate into *polar filaments*. Another set with $\alpha = 0.6\pi$ and $\sqrt{2D_\theta} = 0.8$ where particles form percolating *nematic bands*, see Ref. [23].

*Results.–*A polar filament consists of a chain of particles moving altogether in the same direction. The direction of movement of the chain is given by an incidental leader in the head of the structure. The leader is then followed by a tail of particles. A particle j in the tail reorients its direction of motion $\boldsymbol{e}_j$ according to neighbors it perceives within narrow cone of vision V_j^{att} of aperture angle α. The leader's self-propulsion orientation $\boldsymbol{e}_i$ is determined by rotational diffusion D_θ. Active particles can also scatter away from an obstacle that is perceived within the wide cone of vision V_i^{rep} of aperture angle β, see Fig. 1b. Particles can escape a polar filament due to a strong fluctuation of their self-propulsion orientation, e.g. for high values of D_θ, on encounter with an obstacle, or on encounter with more particles. Collisions of several filaments can also lead to aggregation into a single bulky structure, which does not necessarily consist of a single chain of head-to-tail particles, but can contain many particles in a localized region.

For $N_o = 30$ obstacles, we observe that filaments navigate while trying to avoid obstacles, and furthermore they show to self-trap around an obstacle, see Fig. 1b. Loop formation can occur when the incidental leader of a motile filament starts following the tail. In the presence of obstacles, a loop can be formed from a single polar filament that reorients due to collisions with obstacles, thus leading to a closed polar structure. However, other particles can also join the loop in any direction, thus leading to a final closed nematic structure, where some of the particles in the structure rotate clockwise with respect to the center of the group, and some others rotate counter-clockwise. Once formed, the loop shrinks down arguably due to an effective line tension, then when an obstacle is in the center of the configuration the loop displays self-trapping: the obstacle prevents the loop from shrinking down any further, meanwhile particles still align with their neighbors keeping the loop cohesive, see Fig. 2b. In contrast, when no obstacles are present, the shrinking loop becomes unstable when it reaches a minimum size, then fragments into several polar filaments propagating radially outwards of the loop center, see Fig. 2a. To quantify the shrinking behavior, we compute the radius of gyration R_g with respect to the center of a loop formed by $N = 100$.

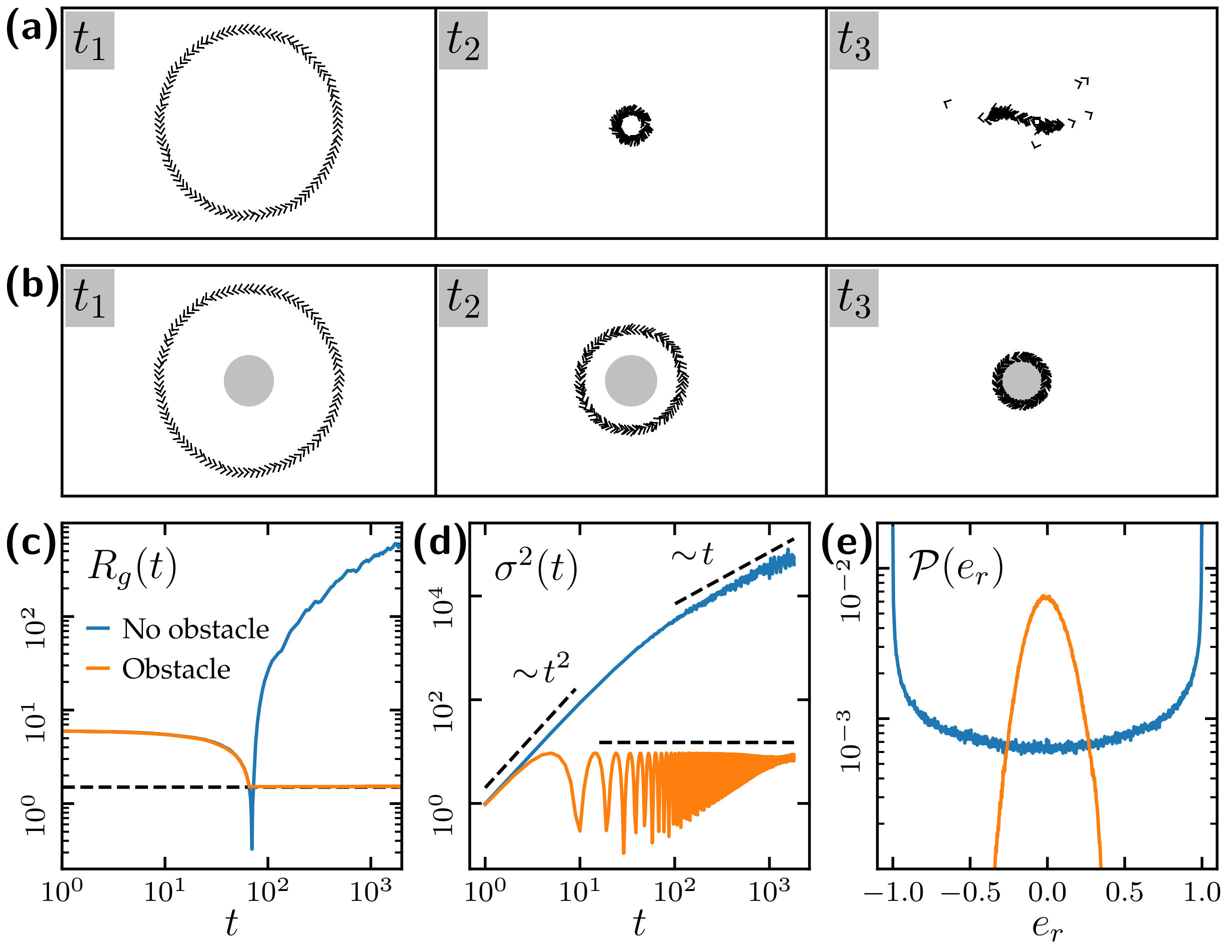

FIG. 2. Loop shrinking. (a) Without an obstacle, the loop shrinks down to a size $r < r_o$, then fragments into several polar filaments that propagate radially out of the center. (b) With an obstacle the loop shrinks down to a size $r = r_o$ and stabilizes around the obstacle. (c,d) Time evolution of dynamic parameters corresponding to configurations in (a,b), namely radius of gyration $R_g(t)$, and mean squared displacement $\sigma^2(t)$. (e) Probability density of finding a particle with radial orientation e_r with respect to the center of the configuration at t_1.

Results in Fig. 2c show that R_g initially decreases both with and without an obstacle. When the loop self-traps around the obstacle R_g reaches a constant value proportional to the size of the obstacle, $R_g \approx r_o$. Without the obstacle, the radius of gyration decreases to a minimum value of $R_g \approx 0.2$, then it diverges at longer times when the loop has lost cohesion forming propagating polar filaments. Moreover, we quantify the mean-squared displacement σ^2, which is found to transition from ballistic to diffusive regime in the case without an obstacle, and displays a plateau in the case with an obstacle. We conclude that self-trapping corresponds to a pinning mechanism that drastically impacts the transport properties of the system. Finally, to quantify the average orientation of the particles in the loop, we obtain the radial orientation component $e_r = \hat{\boldsymbol{e}} \cdot \hat{\boldsymbol{r}}$ for each particle, where $\hat{\boldsymbol{r}}$ is a unitary radial vector with origin at the center of the configuration at time t_1, see Fig. 2a,b. Here, $e_r = 1$ indicates particles are radially outward oriented, and $e_r = -1$ are radially inward oriented, wheres $e_r = 0$ corresponds to tangentially oriented particles. We obtain the probability density $\mathcal{P}(e_r)$, see Fig. 2e. We find that, in the case with an obstacle, $\mathcal{P}(e_r)$ is centered around $e_r = 0$ and vanishes at $e_r = -1, 1$. This shows that trapped particles have an orientation vector mostly tangential to the obstacle with slight deviations corresponding to the width of $\mathcal{P}$. Deviations result from fluctuations due to rotational noise. Conversely, in the case without an obstacle, the maximum occurs at $e_r = -1, 1$ as here particles are mostly propagating radially away from the center of the initial configuration.

We study the order transition of a trapped loop from polar to nematic. Consider an initially polar closed loop. This loop consists of a certain number of active particles that can be rotating either clockwise (CW) or counter-clockwise (CCW). Note that, in contrast to the Vicsek model, the positional-based alignment defined in Eq. (2) does not align orientations of neighbouring particles to be the same. In other words, local order can be either polar or nematic. In Fig. 3a we show a polar loop formed by $N_{\mathrm{CCW}} < N$ particles, i.e. it contains only a fraction of the total particles in the system. As the system evolves, more particles can join the loop, and they can join either in the counter- or clockwise direction. Therefore, an initially polar loop can become nematic over time with N_{CCW} and N_{CW} particles. In Fig. 3b we show the time evolution of the number of particles in the loop. We observe that the number increases over time, with step increases that correspond to incoming bulky filaments that are absorbed by the loop. The loop in this case starts with $N_{\mathrm{CCW}} = 200$, and $N_{\mathrm{CW}} = 0$ particles at $t = 2200$. At a later time $t = 4700$ the loop consists of $N_{\mathrm{CCW}} \approx 500$ and $N_{\mathrm{CW}} \approx 100$ particles. We also compute the time evolution of the local polar order s_1 as well as local nematic order s_2 with the formula

$$s_n = \left| \frac{1}{N} \sum_{i=1}^{N} e^{in\theta_i} \right|. \tag{3}$$

We observe a decrease from $s_1 \approx 0.85$ to $s_1 \approx 0.6$ in the final configuration. The local nematic order s_2 decreases only slightly from $s_2 \approx 0.5$ to $s_2 \approx 0.4$.

We consider a nematic loop of $N = 90$ particles placed at an initial distance of $R_0 = 6$

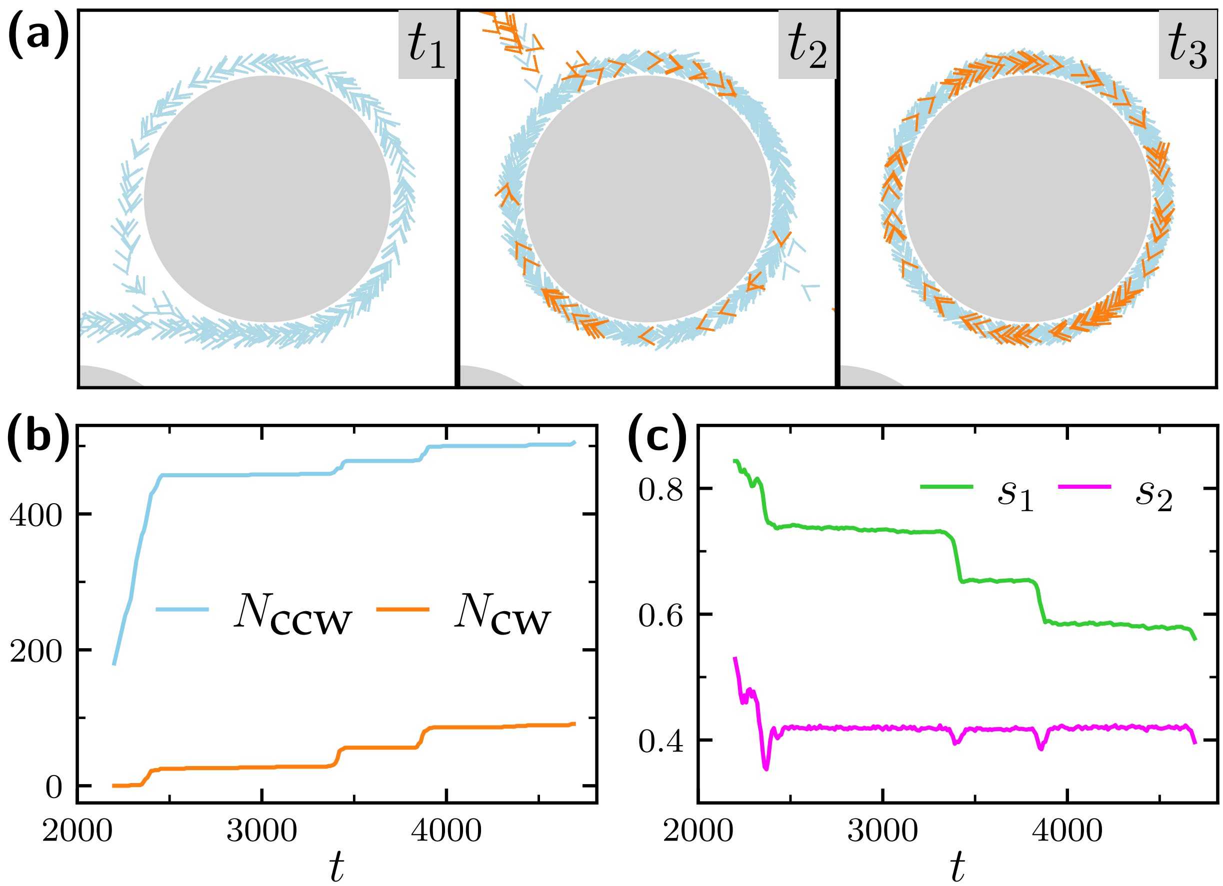

FIG. 3. (a) Transition of the loop from initial polar to final nematic. Time evolution of (b) the number of clockwise N_{CW} and counter-clockwise N_{CCW} particles in the loop, and(c) the local polar order s_1, as well as local nematic order s_2.

from the center of a single obstacle. For the standard parameters considered, namely $v_0 = 1$ and $\gamma = 5$, we obtain that the loop shrinks and gets trapped around the obstacle. We test this scenario for several values of the turning strength γ at $v_0 = 1$, and obtain the radius of gyration R_g for each realization. Results are shown in Fig. 4a. For $v_0 = 1$, we observe that R_g decreases and saturates at longer times when the loop has stabilized around the obstacle, reaching the minimum size of $R_g = 1.5$. For larger values of γ, the radius of gyration shows to decrease more rapidly. Furthermore, for $v_0 = 2$, we observe that with the small turning speed $\gamma = 4$ shown here, R_g monotonously increases in time, indicating that the loop does not shrink in this case, see Fig. 4b. On the contrary, the spread of active particles around the obstacle grows, thus indicating that the loop grows in size instead. For $\gamma = 5$, R_g slowly decreases, and does not saturate for the simulation time here considered. To further

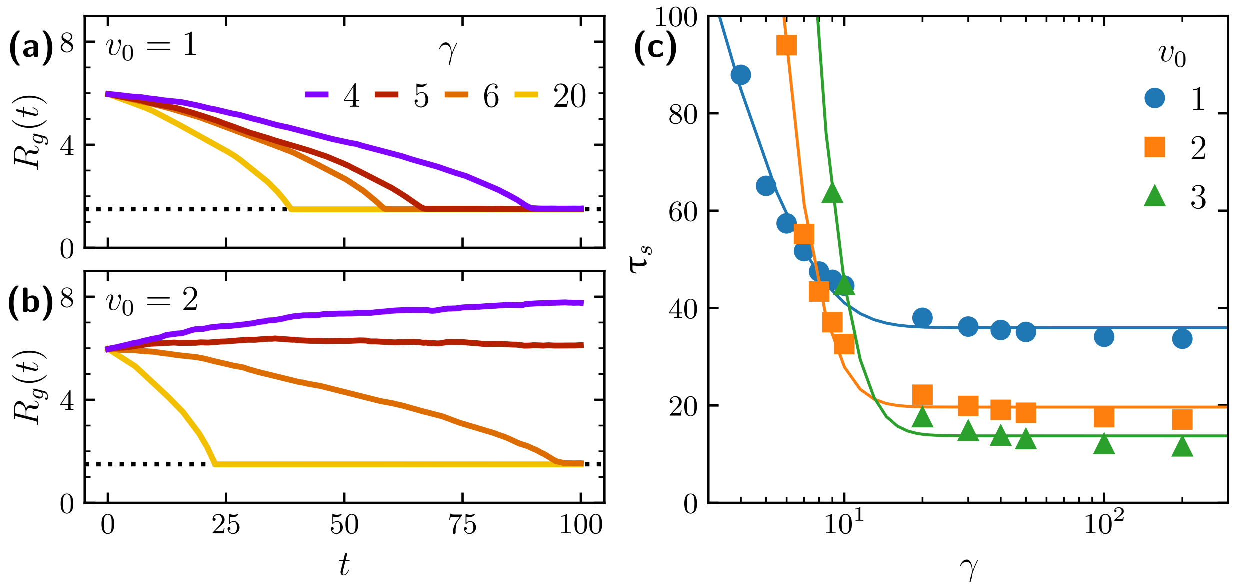

FIG. 4. Radius of gyration for several values of the alignment strength γ and self-propulsion velocity (a) $v_0 = 1$, and (b) $v_0 = 2$. Horizontal dotted line indicates the minimum value $R_g = 1.5$ given by the obstacle size. (c) Shrinking time obtained from (a,b) when the loop reaches minimum size.

characterize the shrinking behavior, we compute the shrinking time τ_s from $R_g(\tau_b) = 1.5$. Obtained values are shown in Fig. 4c, indicating that the shrinking time remains mostly constant for larger values of the turning speed, namely for $\gamma > 10$. However, τ_s significantly increases for smaller values $\gamma < 10$ at any given self-propulsion speed v_0.

In the absence of external disturbances, the stability of a particle loop surrounding an obstacle is not guaranteed. For example, large values of D_θ can also trigger de-trapping, as it directly influences the particle orientation $\boldsymbol{e}$, allowing them to point radially out of the loop configuration. When the aperture angle α of the cone of vision is narrow, particles pointing out of the loop configuration do not perceive other neighbors and do not co-align to join the loop anymore, instead they escape the trap. This can trigger de-trapping of the whole structure, as the escaping particle can serve as an incidental leader which will be followed by the rest of the particles in the loop. To test particle trapping for different parameters of the cone of vision as well as noise strength, we perform simulations of a single loop around one obstacle. We consider several values of α and β, both at low and also high values of the noise strength $\sqrt{2D_\theta}$. See results in Fig. 5. We observe that at low noise, $\sqrt{2D_\theta} = 0.3$, trapping

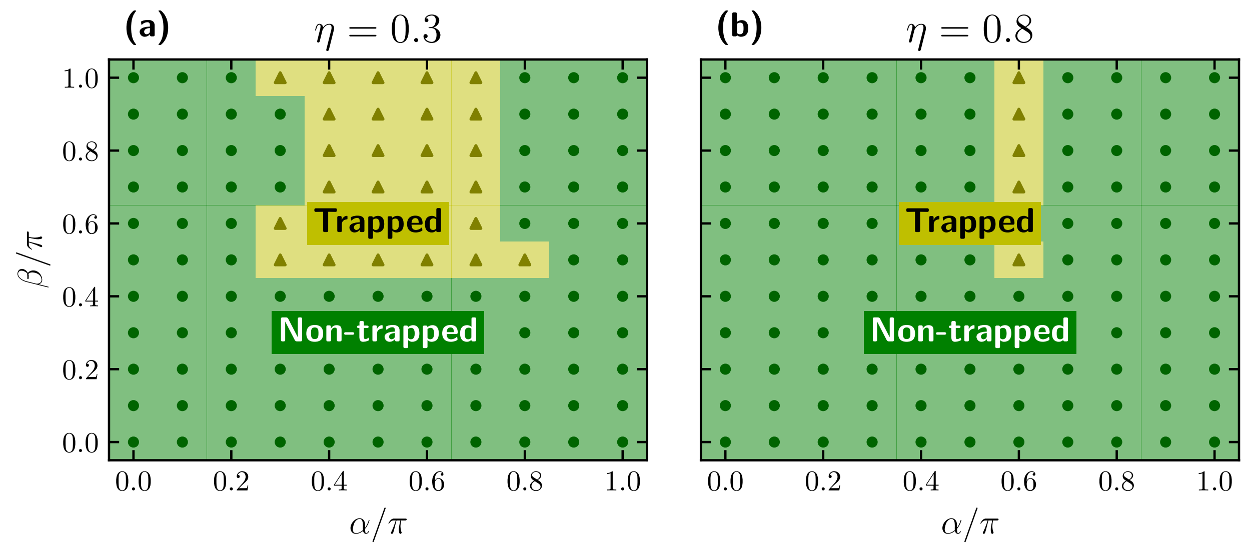

FIG. 5. Single loop trapping diagram for several values of α and β at (a) low noise $\sqrt{2D_\theta} = 0.2$, and (b) high noise $\sqrt{2D_\theta} = 0.8$.

only occurs for large values of the obstacle perception angle $\beta \geq 0.5$, and for intermediate values of the neighbor perception angle α. For high noise, $\sqrt{2D_\theta} = 0.8$, we observe trapping only occurs for $\alpha = 0.6$ and large $\beta = 0.5$.

We obtain the cluster size distribution $P(m)$ by performing a clustering analysis with a cutoff radius of $r_c = 1.5$, such that neighbors are considered to be part of a single cluster only when they are close together a distance $r < r_c$. The clustering analysis is averaged over a time interval of $\Delta\tau = 100$, during which particles are aggregated into a large filament in the case without obstacles $N_o = 0$, or into a dense nematic loop in the case with obstacles $N_o = 30$. Results are shown in 6a. Without obstacles, $P(m)$ shows as a delta distribution around $N = 900$, as well an exponential distribution for clusters of small size $m < 10$. With obstacles, a delta distribution is shown around $N_o = 600$, as well as a power law distribution for clusters of small size $m < 10^2$. We also obtain the marginal displacement probability density $\mathcal{P}(x)$, where each displacement is measured during a time interval of $\Delta t = 15$. Results are shown in 6b. Without obstacles $N_o = 0$, $\mathcal{P}$ shows to be a uniform distribution. With obstacles $N_o = 30$, the marginal displacement PDF shows a quadratic dependence $\mathcal{P} \sim -x^2$ for small displacements which correspond to the trapped particles in the nematic loop. Moreover, for larger displacements a Gaussian-like dependence is shown.

A percolating *nematic band* is formed due to a reorientation mechanism similar to the

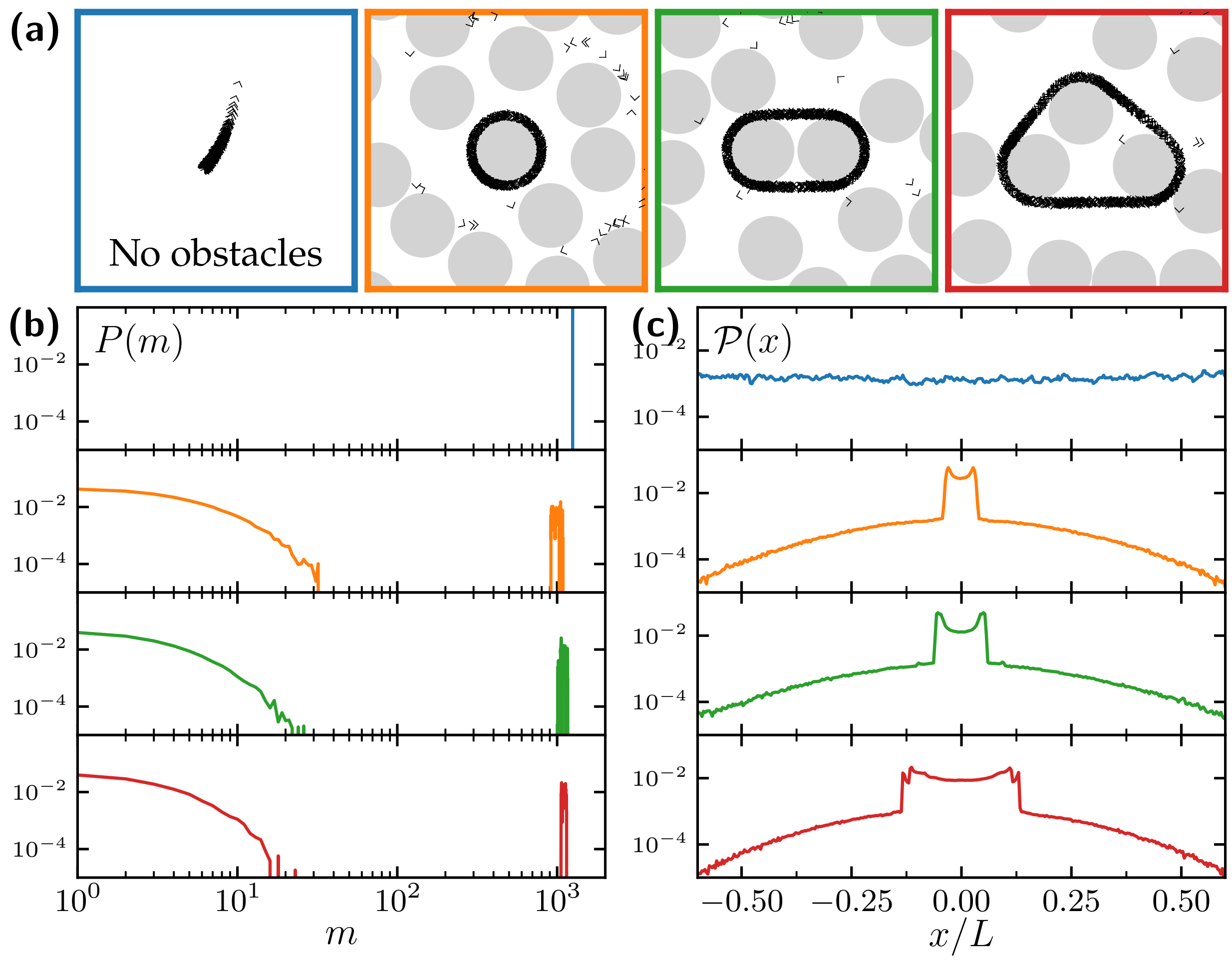

FIG. 6. (a) Polar filament found in the case without obstacles, and closed loops for self-trapping around 1, 2, and 3 obstacles. (b) Cluster size distribution $P(m)$, and (c) marginal displacement probability density $\mathcal{P}(x)$ for $N_o = 0, 30$. Cases considered correspond to those in panel (a). For $P(m)$ a clustering analysis is performed with a cutoff radius of $r_c = r_o$. For $\mathcal{P}(x)$, displacements are calculated during a time interval of $\Delta t = L/v_0$.

filaments case, however here the particles can reorient and reverse their direction due to the broader vision cone aperture angle $\alpha = 0.6$. Over time the band tends to rectify and percolate, as described in Ref. [23]. However, in the presence of obstacles, a band can find its way around an obstacle. In some cases, the bands won't percolate, but the structure might close within itself, forming a nematic loop enclosing multiple obstacles, see Fig. 7.We obtain local polar and local nematic order parameters, s_1 and s_2, respectively. For parameters (α, D)=(0.3π,0.3) corresponding to filaments, we observe that s_1 monotonously decreases with the number of obstacles N_o, see Fig. 8a. Without obstacles particles ag-

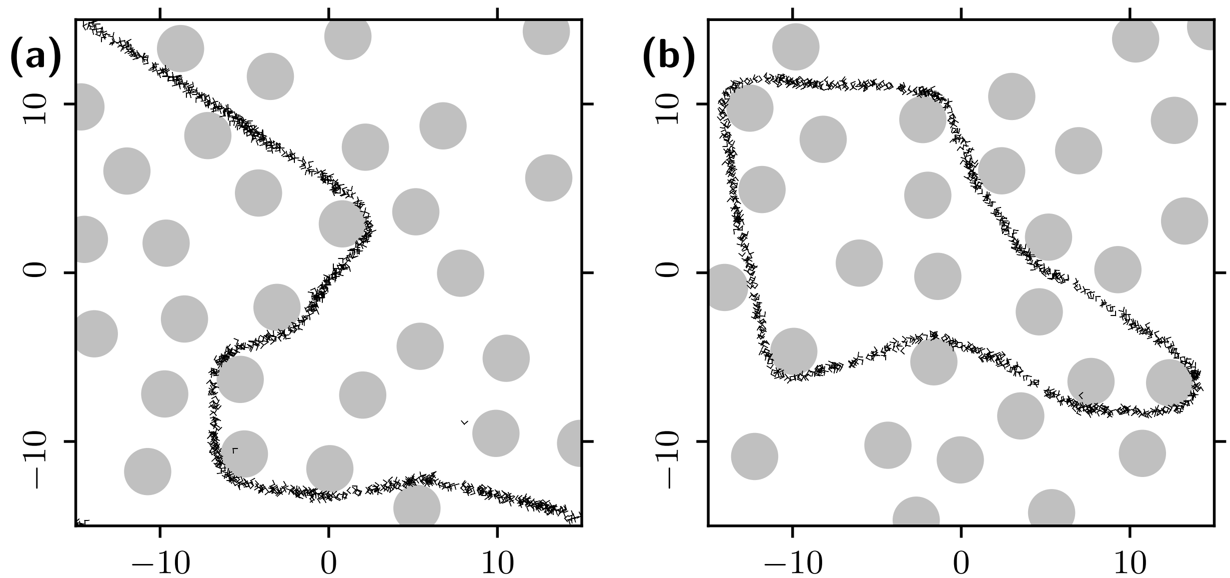

FIG. 7. Representative snapshots of nematic bands formed for two different obstacle configurations where the band is (a) percolated, and (b) forming a closed loop around several obstacles.

gregate into a single dense filament, and with increasing number of obstacles the filament has a larger probability of fragmenting, which explains the decrease in polar order. For $(\alpha, \sqrt{2D_\theta})$=(0.3$\pi$,0.3) corresponding to bands, s_1 remains zero at any N_o, as in this case the bands are nematic due to the local interaction of between particles. Furthermore, the local nematic order parameter s_2 shows monotonously decrease both for filaments and bands, see Fig. 8b. Note that local polar order contributes to the overall value of s_2. For this reason, filaments show the same behavior for both s_1 and s_2, with slightly larger values of s_2 at larger N_o, as nematic loops appear for higher N_o. For bands, s_2 is non-vanishing and shows to decrease with increasing N_o, indicating the effect of obstacles is to diminish local nematic order due to the bending around obstacles.

Discussion.–Self-trapping of polar filaments depends on the parameters of the cone of vision α, and β. Such perception parameters are intrinsic to the particle and independent of the obstacle configuration. In a configuration of homogeneously distributed obstacles like the one employed here, particles have the same probability to self-trap around any of the obstacles. However, a non-homogeneous configuration can be considered in order to fabricate a filter [11]. When trapping occurs, the loops become absorbent and a pinning behavior is induced. Interactions between conspecifics lead to localized nematic alignment

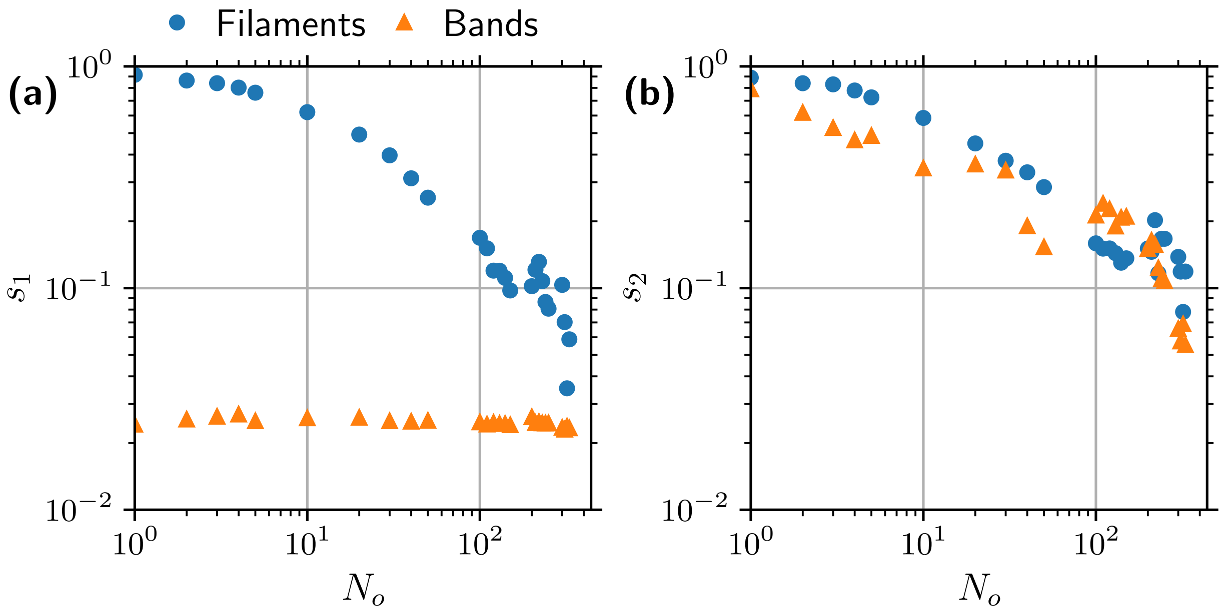

FIG. 8. Steady state local order parameters for bands and filaments with varying number of obstacles N. (a) Local polar order. (b) Local nematic order.

within the loops. Note that these interactions do not favor any type of local order (polar or nematic), instead they tend to influence the orientations of the particles towards regions of higher particle density. Trapped loops can destabilize due to different mechanisms, like external filaments passing by or joining the loop, as well as fluctuations given by rotational diffusion D_θ. Stability can depend on the size of the loops, as well as the number of surrounded obstacles. Noise is also an important parameter, which is already known to change the collective behaviour of the active particles to transition from polar filaments to nematic bands, and even to form aggregates at higher values [23]. Trapping around multiple obstacles is more likely to be observed for intermediate values of the noise, which corresponds to nematic bands. However, bands are also likely to percolate, and it is still to be verified whether this is a finite-size effect, or truly long-range order.

Our results corresponds to a first examination of the effects of crowded environments in active particles with non-reciprocal interactions. Self-trapping is a novel effect emerging from perception parameters, which could be present in animals that interact through visual perception, or bacteria with non-reciprocal interactions.

This work was financially supported by the CONACYT-DAAD scholarship program.

* rsaavedra@cicese.mx

† fernando.peruani@cyu.fr

[1] L. Bruno, M. Salierno, D. E. Wetzler, M. A. Despósito, and V. Levi, PLOS ONE **6**, e18332 (2011).

[2] K. Barlan and V. I. Gelfand, Cold Spring Harb. Perspect. Biol. **9**, a025817 (2017).

[3] J. D. Partridge and R. M. Harshey, J. Bacteriol. **195**, 909 (2013).

[4] A. Yang, W. S. Tang, T. Si, and J. X. Tang, Biophys. J. **112**, 1462 (2017).

[5] E. Altshuler, G. Miño, C. Pérez-Penichet, L. del Río, A. Lindner, A. Rousselet, and E. Clément, Soft Matter **9**, 1864 (2013).

[6] N. Figueroa-Morales, G. L. Miño, A. Rivera, R. Caballero, E. Clément, E. Altshuler, and A. Lindner, Soft Matter **11**, 6284 (2015).

[7] J. Nguyen, J. Lara-Gutiérrez, and R. Stocker, FEMS Microbiol. Rev. **45**, fuaa068 (2020).

[8] R. G. Seidler, R. A. Long, J. Berger, S. Bergen, and J. P. Beckmann, Biol. Conserv. **29**, 99 (2015).

[9] M. Leclerc, M. Leblond, M. Le Corre, C. Dussault, and S. D. Côté, J. Mammal. **102**, 1342 (2021).

[10] J. Codina, B. Mahault, H. Chaté, J. Dobnikar, I. Pagonabarraga, and X.-q. Shi, Phys. Rev. Lett. **128**, 218001 (2022).

[11] O. Chepizhko and F. Peruani, Phys. Rev. Lett. **111**, 160604 (2013).

[12] O. Chepizhko, E. G. Altmann, and F. Peruani, Phys. Rev. Lett. **110**, 238101 (2013).

[13] Z. Mokhtari and A. Zippelius, Phys. Rev. Lett. **123**, 028001 (2019).

[14] B. Zhang, F. Tan, and N. Zhao, Soft Matter **17**, 10334 (2021).

[15] L. Theeyancheri, S. Chaki, T. Bhattacharjee, and R. Chakrabarti, Phys. Rev. E **106**, 014504 (2022).

[16] A. Dinelli, J. O'Byrne, A. Curatolo, Y. Zhao, P. Sollich, and J. Tailleur, Nat. Commun. **14**, 7035 (2023).

[17] M. Durve, A. Saha, and A. Sayeed, Eur. Phys. J. E **41**, 49 (2018).

[18] Z. You, A. Baskaran, and M. C. Marchetti, PNAS **117**, 19767 (2020).

[19] M. Fruchart, R. Hanai, P. B. Littlewood, and V. Vitelli, Nature **592**, 363 (2021).

[20] K. L. Kreienkamp and S. H. L. Klapp, New J. Phys. **24**, 123009 (2022).

[21] M. Knežević, T. Welker, and H. Stark, Sci. Rep. **12**, 19437 (2022).

[22] J. P. Newman and H. Sayama, Phys. Rev. E **78**, 011913 (2008).

[23] L. Barberis and F. Peruani, Phys. Rev. Lett. **117**, 248001 (2016).

[24] P. Stengele, A. Lüders, and P. Nielaba, Phys. Rev. E **106**, 014603 (2022).

[25] J. Qi, L. Bai, Y. Xiao, Y. Wei, and W. Wu, Inf. Sci. **582**, 850 (2022).

[26] R. S. Negi, R. G. Winkler, and G. Gompper, Soft Matter **18**, 6167 (2022).

[27] R. S. Negi, R. G. Winkler, and G. Gompper, Phys. Rev. Research **6**, 013118 (2024).

[28] F. Ginelli, F. Peruani, M.-H. Pillot, H. Chaté, G. Theraulaz, and R. Bon, Proc. Nat. Acad. Sci. **112**, 12729 (2015).

[29] R. Martinez, F. Alarcon, D. R. Rodriguez, J. L. Aragones, and C. Valeriani, Eur. Phys. J. E **41**, 91 (2018).

[30] F. A. Lavergne, H. Wendehenne, T. Bäuerle, and C. Bechinger, Science **364**, 70 (2019).

[31] J. Qi, L. Bai, Y. Xiao, W. Wu, and L. Liu, IEEE Access **8**, 160490 (2020).

[32] C.-J. Chen and C. Bechinger, New J. Phys. **24**, 033001 (2022).

[33] Cs. Sándor, A. Libál, C. Reichhardt, and C. J. Olson Reichhardt, Phys. Rev. E **95**, 032606 (2017).

[34] J. Toner, N. Guttenberg, and Y. Tu, Phys. Rev. Lett. **121**, 248002 (2018).

[35] S. Kumar and S. Mishra, Phys. Rev. E **106**, 044603 (2022).

[36] Y. Duan, B. Mahault, Y.-q. Ma, X.-q. Shi, and H. Chaté, Phys. Rev. Lett. **126**, 178001 (2021).